Journal of Colloid and Interface Science 638 (2023) 743–757

Contents lists available at ScienceDirect

Journal of Colloid and Interface Science

journal homepage: www.elsevier.com/locate/jcis

Computational assessment of hexadecane freezing by equilibrium atomistic molecular dynamics simulations

Stoyan Iliev [b], Sonya Tsibranska [a,*], Anela Ivanova [b,*], Slavka Tcholakova [a], Nikolai Denkov [a]

[a] Department of Chemical and Pharmaceutical Engineering, Faculty of Chemistry and Pharmacy, University of Sofia, 1 James Bourchier blvd., 1164 Sofia, Bulgaria
[b] Department of Physical Chemistry, Faculty of Chemistry and Pharmacy, University of Sofia, 1 James Bourchier blvd., 1164 Sofia, Bulgaria

GRAPHICAL ABSTRACT

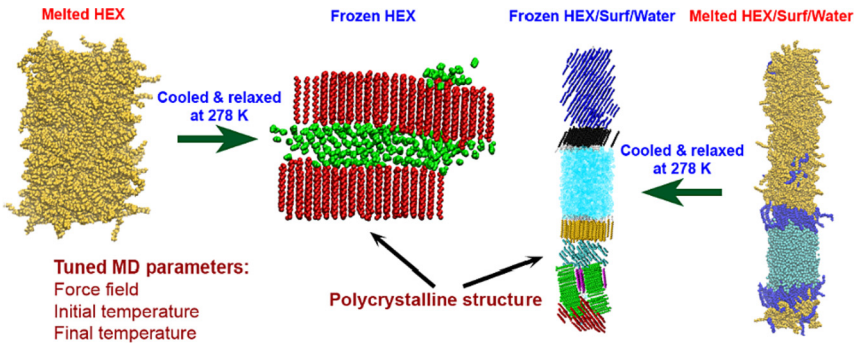

ARTICLE INFO

Article history:
Received 5 December 2022
Revised 3 January 2023
Accepted 25 January 2023
Available online 31 January 2023

Keywords:
Hexadecane
Crystallization
Rotator phases
Molecular dynamics
Solid-state intermolecular organization

ABSTRACT

Hypothesis: Upon cooling, alkanes can form intermediate phases between liquid and crystal. They are called "rotator" or "plastic" phases and have long-range positional order with rotational freedom around the long molecular axis which gives them non-trivial and useful visco-plastic properties. We expect that the formation and structure of rotator phases formed in freezing alkanes can be understood much deeper by tracking the process at molecular level with atomistic molecular dynamics.

Simulations: We defined an appropriate CHARMM36-based computational protocol for simulating the freezing of hexadecane, which contained a sufficiently long (500 ns) equilibrium sampling of the frozen states. We employed it to simulate successfully the freezing of bulk and interface-contacting hexadecane and to provide a pioneering clarification of the effect of surfactant on the crystallization mechanism and on the type of intermolecular ordering in the crystallites.

Findings: The devised computational protocol was able to reproduce the experimentally observed polycrystalline structure formed upon cooling. However, different crystallization mechanisms were established for the two types of models. Crystallites nucleate at random locations in the bulk and start growing rapidly within tens of nanoseconds. In contrast, the surfactants freeze first during the fast cooling (<1 ns), followed by rapid hexadecane freezing, with nucleation starting along the entire surfactant adsorption layer. Thereby, the hexadecane molecules form rotator phases which transition into a more stable ordered phase. This collective transition is first-time visualized directly. The developed robust computational protocol creates a foundation for future in-depth modelling and analysis of solid-state alkane-containing, incl. lipid, structures.

* Corresponding authors.s.
E-mail addresses: st@lcpe.uni-sofia.bg (S. Tsibranska), aivanova@chem.uni-sofia.bg (A. Ivanova).

https://doi.org/10.1016/j.jcis.2023.01.126
0021-9797/

1. Introduction

Alkanes and their mixtures have a remarkable and non-trivial physical property - they form intermediate structural phases between the isotropic liquid and the regularly ordered solid crystalline phase [1,2]. These intermediate phases are usually called "rotator phases" or "plastic phases" because the alkane molecules therein retain considerable freedom in terms of molecular rotation, although they have long-range positional order in three-dimensional space (as in a real crystal lattice) and exhibit complex visco-plastic rheological behaviour [3].

Rotator phases have some unique features, leading to surface freezing instead of the more typical surface melting of solids. Various phenomena and characteristics related to rotator phases were studied, incl. crystal nucleation, entropy and enthalpy of crystallization, surface energy between the crystal and its melt, entropy and enthalpy of phase transition in surface layers, etc. [1,4,5]. All these phenomena are very important in the context of applications of alkanes [6], as well as in the understanding and analysis of phase transitions in lipid molecular assemblies in biosystems, such as bio-membranes and lipid vesicles [1,7].

The newly observed phenomena of "self-shaping" and "self-bursting" are also related to the presence of rotator phases in alkane drops [8–12]. In alkane-in-water emulsions, a spontaneous change in the droplets shape is observed upon existence of rotator phases [13]. These phenomena can be used to construct complex hierarchical supramolecular structures [8,9,12]. Currently, five rotator phases (denoted as R_I to R_V) are registered for alkanes [9], differing by the intermolecular arrangement and by the tilt of the molecules with respect to the crystal plane.

Thermodynamically stable rotator phases are observed in bulk alkanes with odd number of carbon atoms in the chain at 11 or more C atoms [1,14]. For bulk alkanes with even number of carbon atoms, thermodynamically stable rotator phases are registered for representatives with 22 C atoms or more [14]. This difference in the minimum chain length for the formation of stable rotator phases in bulk alkanes reveals the important role of molecular symmetry and packing in the alkane crystallization. This is also reflected in the crystal lattices of alkanes. Even-numbered alkanes with a chain length between 14 and 24 C atoms form a triclinic crystal lattice, between 26 and 38 C atoms – a monoclinic one, and between 40 and 66 C atoms – an orthorhombic crystal lattice [15]. Conversely, odd alkanes with a chain length between 13 and 41 C atoms freeze in an orthorhombic lattice, while shorter-chain odd number alkanes crystallise in a triclinic space group [15].

Micro- and nano-confinements can significantly change the phase transition temperatures and the stability of the phases formed [13]. The confinement strongly influences the crystallization and the formation of intermediate rotator phases. Phases observed only with bulk long-chain alkanes may appear stable or metastable in confined spaces for much shorter alkanes. Both the confinement geometry (pores, microcapsules, emulsion drops) and the chemical nature of the confinement wall (for emulsions, the type of surfactant adsorbing on the alkane drop surface) can affect the phase behaviour of alkanes. The presence of confinement and surface curvature also influences the type and rate of crystallization. The surface nucleation mechanism is activated and crystallization rates are much higher when rotator phases are formed [16,17]. All these studies show that surfactants in the adsorption layer and surface curvature play an important role in the formation of rotator phases in emulsion drops [17].

The rotator phases are extensively studied experimentally but at the molecular level many questions remain unanswered because of limitations in the resolution of the experimental techniques. Hence, molecular modelling would be very helpful to deepen our knowledge about these interesting but complex structures and the related phenomena.

The properties of rotator phases are described in a number of molecular simulation studies [18–40] (see also the Supporting Information, Section: Overview of molecular simulations studying rotator phases of alkanes). Ryckaert et al. [23,24] performed atomistic MD simulations of shorter chains and confirmed the importance of the longitudinal translation for the rotator phases. The latter were effectuated by 90° flips of the molecules about their long axes. The separate molecules were reported to be in *all-trans* conformation and to have mobile chain ends. Frank and van der Merwe [41] proposed that the rotation of a given alkyl chain could occur by a soliton-like step-by-step propagation of a dihedral kink defect down the chain. This type of motion was observed also in the work of Doherty and Hopfinger [42] and of Milner et al. [39]. Guillaume et al. [43] introduced the orientations of the molecules with respect to the *ab* plane as an order parameter to characterize the intermolecular packing.

Cao et al. [34] unveiled that the $R_{II} - R_I$ phase transition was first-order. Stable triclinic structure and rotator phase for the odd-parity alkanes was observed, while for the even-parity ones shorter than C_{20} the triclinic crystalline structure was stable but the rotator phase was not. Wentzel et al. [37,38] tested several all-atom potentials and found that the results with a Flexible Williams force field [44] were closer to the experimental data. Rotator phases in odd-parity alkanes were found to be stable in a wide temperature range but the relative stability of the possible crystal lattices was not predicted accurately.

Rao et al. [45,46] suggested the diffusion and heat capacity of normal alkanes and their mixtures as indicators, which may be used to determine the melting point. Tsuchiya et al. [47,48] proposed radial distribution functions of the carbon atoms as a sensitive melting point indicator. Burrows et al. [49] compared the accuracy of seven different force fields (all-atom, united-atom and coarse-grained) for describing liquid-to-solid and solid-to-liquid phase transitions in normal alkanes. Most of the force fields were modified in order to reproduce better the properties of the modelled systems. The mass fraction of the crystalline phase was adopted as a criterion for melting. The melting point was considered to be the temperature at which the smallest change in the densities of the liquid and crystalline phases upon melting was registered. Mass densities of the liquid alkanes yielded by the CHARMM36, L-OPLS and Williams 7B force fields corresponded best to the experimantal values. For $C_{15}H_{32}$ and $C_{16}H_{34}$, the diffusion coefficient was best reproduced by CHARMM36, and for C_8H_{18} Williams 7B performed best. For $C_{15}H_{32}$, all atomistic force fields predicted a transition from a herringbone arrangement to a monoclinic phase, which is inconsistent with experiments. This was also observed by Wentzel & Milner [38]. The transition from crystalline phase to R_I was accomplished only by COMPASS and Williams 7/7B. For $C_{16}H_{34}$, all atomistic force fields reproduced the formation of a triclinic crystal phase. Bratek et al. also benchmark the ability of a set of force fields to compute properties of *n*-pentadecane in liquid (298 K) and solid (277 K) state [50]. They conclude that CHARMM36 and the newest version of OPLS reproduce well most of the properties in the two physical states.

In summary, both pure alkanes and mixtures are theoretically studied by molecular simulations. Procedures are developed to predict the solid-to-liquid transition temperature from the self-diffusion coefficient and heat capacity [45] and also from a change in the profile of the radial distribution function of the carbon atoms in the system [47]. The transitions of $C_{23}H_{48}$ from crystal phase to R_I, from R_{II} to R_I and back are also described, using specially devel-

oped order parameters [37]. MD simulations of $C_{18}H_{38}$, $C_{19}H_{40}$ and $C_{20}H_{42}$ close to their melting temperatures are performed. In $C_{19}H_{40}$, a spontaneous transition from crystalline phase to R_I is observed, initiated by correlated "jumps" of molecules along their long axis and rotation of the molecules by 90° about this axis [36]. In the case of even alkanes, the formation of R_I and R_{II} phases is observed. MD simulations are complemented by NMR and IQNS experiments that investigate the structure of the R_I phase of $C_{19}H_{40}$ [43]. The accuracy of seven different force fields for describing phase transitions in normal alkanes is compared, as well as the ability to predict melting points, density and self-diffusion coefficients [49]. From the results summarised briefly above, it can be concluded that none of the potentials can predict all properties of the studied alkanes, while CHARMM36, COMPASS and Williams 7 give acceptable estimates.

The results from MD simulations described so far are in most cases based on relatively short simulations, from 10 ps [21] to 20 ns [49] equilibrium trajectories, with only one report analysing 100 ns to 300 ns MD runs [50]. Most often, the simulations start from crystalline phase and the change during melting is studied [e.g. 23, 24, 40] because such an approach is much faster. However, when studying alkanes with even number of carbon atoms in the chain (shorter than C_{20}), it is important to track the cooling process because rotator phases are observed experimentally in these systems upon cooling only [13]. In some instances [45,46,49], averaged thermodynamic characteristics are presented but the system is not in equilibrium either due to short simulation time or to the choice of computational protocol which involves constant temperature change in the system, thus contradicting the concept of equilibrium molecular dynamics (MD). In addition, simulations of alkanes in the presence of surfactants and water have not been carried out yet.

The current work aims at elucidating further the molecular mechanisms of freezing of alkane-containing systems with special focus on the detection and characterization of rotator phases therein. We perform equilibrium molecular dynamics simulations of bulk hexadecane and hexadecane/surfactant/water mixture, the latter being simulated upon freezing for the first time. We test four different all-atom force fields and select the most appropriate one for the subsequent computations by demonstrating through comparison to experimental data that it is able to reproduce the key features of the phase transition. The temperature of phase transition upon cooling, the effect of initial and final temperature, and the molecular structure after freezing are clarified. The nucleation mechanism and its dependence on the presence of surfactants is highlighted, which lacks in previous studies. As another novelty, a collective transition of the alkane molecules from an initial rotator phase to a more ordered state is registered and visualized.

2. Molecular models and computational protocol

Two types of model systems are investigated in this study. The first one is bulk hexadecane (denoted further on as bulk HEX) consisting of 440 molecules (22000 atoms). The second one contains 494 molecules hexadecane, 108 surfactant $C_{16}(EO)_2$ molecules and 2778 water molecules (HEX/Surf/water model, ≈43000 atoms) arranged at a flat interface (Fig. 1).

The starting structures of both systems are ordered. The molecules are placed on the nodes of a regular hexagonal lattice and each of them is rotated randomly about the long molecular axis to accelerate melting. The initial area per molecule is 0.195 nm^2 and corresponds to the experimental value for triclinic crystal hexadecane [13,51]. The model of bulk HEX consists of four layers along the *c* direction (which coincides with the *z* axis of the periodic box). Each layer contains 110 molecules – 11 in each row

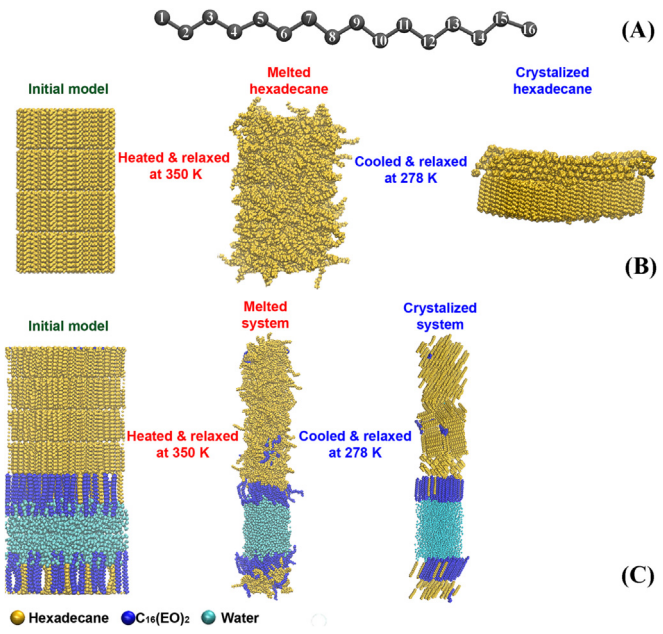

Fig. 1. (A) Carbon skeleton of hexadecane with numbering of the atoms. The same numbering applies for the carbons in the alkyl chain of the surfactant; the gray arrow denotes the vector C3-C13 (see text); illustration of the simulated molecular models of (B) bulk HEX and (C) HEX/Surf/water.

along the *x* direction and 10 along *y*. The initial configuration of the HEX/Surf/water model consists of the same hydrocarbon construct, appended to a symmetric surfactant/water/surfactant slab. The mirrored adsorption layers (Fig. 1, bottom left) are built of rows of alternating hexadecane and $C_{16}(EO)_2$ molecules (as proposed in Ref. 9). Due to the lack of experimental data for this particular system, an initial HEX:Surf ratio of 1:2 was chosen. It may then self-adjust during the melting within the chosen computational setup. The molecules in the initial adsorption layers are also evenly spaced. The hydrophilic heads of the surfactants are solvated with water molecules taken from a standard liquid water box equilibrated at 300 K. The initial thickness of the water slab is 4.5 nm.

A hexagonal periodic box is used for all simulations with initial dimensions 5.2 × 4.5 × 9 nm for bulk hexadecane and 5.2 × 4.5 × 17.2 nm for the hexadecane/surfactant/water system. Periodic boundary conditions are applied in all directions.

The energy of the two model systems is minimised first. Then, they are heated to 350 K with a rate of 1 K/ps in NVT ensemble and equilibrated for 200 ns in NPT ensemble (P = 1 bar) at the final temperature. After this stage, we achieved fully isotropic liquid, which was chosen as initial configuration for subsequent MD simulations. In the next step, the systems are cooled down to 300 K or to 273 K at the same rate of 1 K/ps. We performed also cooling to different temperatures below 300 K, but in this case we used as an initial configuration the final snapshot (at 200 ns) from the simulations at 300 K. At all tested final temperatures, we perform production simulations of 200 ns after the cooling except for the systems at 278 K, for which 500 ns long trajectories are generated. For the simulations at 278 K, three independent trajectories with different initial velocities are generated for each of the two model systems. No changes are witnessed and the results discussed below are representative of the behaviour in all independent runs.

An NPT ensemble with isotropic pressure scaling is used in the production stage for bulk hexadecane and with semi-isotropic pressure scaling for HEX/Surf/water. These types of pressure scaling follow the recommendations of numerous soft matter molecular dynamics simulations from the last two decades of bulk molecular systems (normally simulated with isotropic pressure

scaling) and of lipid bilayers solvated with water (for which semi-isotropic coupling is used), respectively. The thermostat and barostat are v-rescale [52] with a coupling constant of 0.1 ps and Berendsen [53] with a coupling constant of 0.8 ps, respectively. Compressibility of 7.3×10^{-5} bar^{-1} [54] is assigned in all directions of space. The Berendsen barostat is selected because it allows semi-isotropic pressure coupling for the surfactant-stabilized interface and is a very conceptually and numerically stable barostat. It is almost the only alternative, which would ensure consistent pressure coupling before, during and after a phase transition. The Parrinello-Rahman barostat [55] with the same types of pressure coupling for the two model systems (isotropic for bulk HEX and semi-isotropic HEX/Surf/water) or with fully anisotropic scaling was also tested by performing 500 ns equilibrium simulations at 278 K (maintained with a Nosé-Hoover thermostat [56]) of the systems cooled down to this temperature. However, all models remained in the liquid state and no phase transition was observed. Therefore, the Berendsen barostat was retained for all simulations.

The potential for the van der Waals interactions is Lennard-Jones and it is truncated at a distance of 1.2 nm with a switching function activated at 1 nm. The electrostatic interactions are calculated with PME [57–59], where the real-space summation is truncated at 1.2 nm with a switching function turned on at 1.0 nm. The reciprocal-space part is fit by a fourth-order polynomial using B-spline with a Fourier grid spacing of 0.12 nm. The time step is 2 fs and the equations of motion are integrated with leap-frog. The lengths of all hydrogen-containing bonds are fixed with LINCS [60] and those in water – with SETTLE [61]. Coordinates are written every 10 ps to the trajectory file.

We tested four different all-atom force fields: CHARMM36 [62], Lipid17 [63], AMBER99 [64] and OPLS-AA [65] in combination with TIP4P [66,67] water model. We select these force fields because they are parameterised for a large set of lipids, with special focus on the description of the alkyl tails. The L-OPLS [68] force field has been shown to provide accurate results for lipid-containing systems. However, it required some empirical readjustment of atomic charges in order to reproduce a phase transition in bulk pentadecane. Such readjustment of charges would not be straightforward in heterogeneous systems such as HEX/Surf/water and, therefore, we preferred to perform the tests with the standard OPLS-AA force field.

The starting structure for the simulations with each force field was identical. The same computational protocol as described above was applied for all force fields.

The simulations are carried out with the program package Gromacs 2020 [69]. VMD 1.9.4 [70] is used for visualization of the trajectories.

3. Results and discussion

To characterise the phase transition in the model systems, a set of thermodynamic parameters was monitored. A procedure to isolate the multiple ordered domains (crystallites) formed during freezing was developed. To determine the types of ordered phases obtained in the simulations, several structural analyses were made: intermolecular radial distribution functions (RDF), deuterium order parameters of the alkyl chains, 2D Voronoi analysis [71,72], and tilt angle of the molecules relative to the crystallite plane (Supporting Information, Section: Calculation of tilt angles within crystallites, Figures S1-S4).

4. Testing of atomistic force fields

Four different all-atom force fields (CHARMM36 [62], Lipid17 [63], AMBER99 [64] and OPLS-AA [65]) are tested to determine which of them would describe most accurately the phase changes in the model systems (Figure S5). A few criteria were set: (i) a phase transition from regular lattice to isotropic liquid had to be observed when heating the systems to 350 K; (ii) freezing had to take place after cooling the systems to various temperatures between 273 K and 300 K; (iii) the density of the system had to reproduce the experimental data in the liquid state.

The experimental data for the density [73] were reproduced almost quantitatively by CHARMM36 (Fig. 2). This force field also provided densities of the liquid matching those of previous MD simulations [49]. Moreover, this force field was the only one with which all phase transitions were observed, from regular lattice to isotropic liquid and then to an ordered phase at low temperature. The latter is evidenced by the abrupt jump in density between 280 K and 278 K. This jump was observed in both types of models. None of the other force fields was able to capture both transitions (Figure S5). OPLS and AMBER could not achieve the initial solid-to-liquid transition. None of the systems was melted when heated to 350 K. In order to find the temperature where the system melted with AMBER, bulk HEX was heated even up to 1000 K but it could not be liquefied. In contrast, Lipid17 successfully melted the system. However, the hydrocarbons modelled with it could not undergo the transition to an ordered phase at any of the investigated low temperatures.

Since CHARMM36 is the only force field which was able to describe the model systems both qualitatively and quantitatively, it was used for the rest of the simulations. Due to the good correspondence of the density with the experimental value, it may be assumed that this classical potential may be utilized to estimate bulk thermodynamic characteristics of alkane-rich systems. This is in agreement with the conclusions made in a recent study of Glova et al. [74]. They benchmark by MD a series of all-atom and united-atom force fields by modelling bulk *n*-eicosane and comparing its properties to experimental data. It is concluded that CHARMM36 represents very well the structural and thermodynamic, incl. mass density, characteristics of this alkane in a wide temperature range (450 K to 250 K).

The success of CHARMM36 over the other biomolecular force fields is most probably due to the following reasons: (i) its parameters were specifically tuned to represent the intermolecular arrangement of lipid supramolecular assemblies in *various phase states*; (ii) the derivation of the parameters in CHARMM relies on proper balance of *solute–solute and solute–solvent* intermolecular interaction energies; (iii) the torsional potentials for the lipid tails in CHARMM are carefully parameterised in terms of *massive conformational averaging* and reproduction of quantum mechanically generated *trans/gauche interconversion energy profiles*; (iv) *electrostatics is somewhat more dampened* because of the use of partial atomic charges from semi-empirical calculations. Therefore, CHARMM36 is employed for all subsequent simulations.

First, bulk HEX was cooled down with CHARMM36 from 300 K to several different temperatures to check whether freezing took place. It was confirmed that the phase transition occured irrespective of the final temperature as long as it was 278 K or lower. Thereby, crystallites were formed and it should be noted that similar total mass density of the frozen system was obtained at each final temperature.

5. Physicochemical parameters – temperature, enthalpy and density

Several thermodynamic properties of the systems were monitored, which are important for the phase transition, namely, the temperature, enthalpy, and density (Fig. 3).

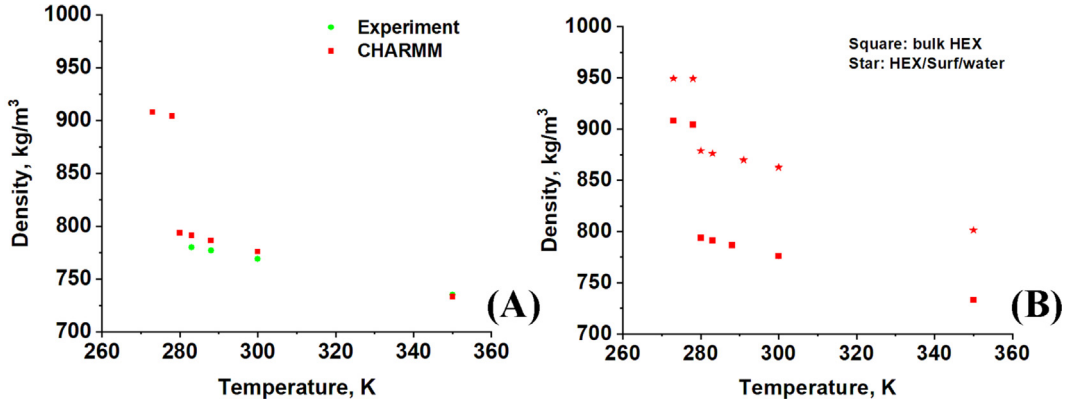

Fig. 2. Density of the entire model systems at different temperatures averaged for the last 20 ns of the respective MD trajectory with CHARMM36 force field: (A) bulk HEX and (B) HEX/Surf/water; the experimental data are from Ref. 73.

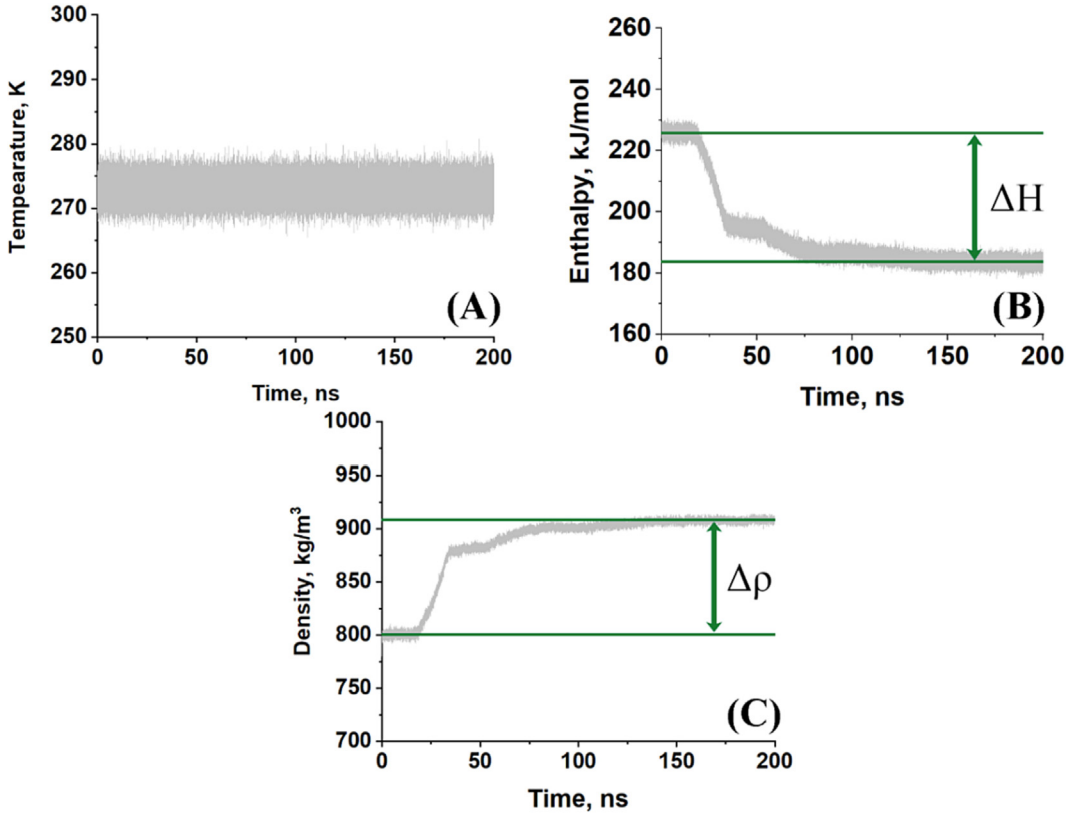

Fig. 3. Illustrative evolution of physical–chemical parameters during crystallization of bulk HEX after cooling from 300 K to 273 K: (A) temperature, (B) enthalpy and (C) mass density.

A sharp change in the enthalpy and density is observed upon freezing in all cases. This change is indicative of first order phase transition in the two types of systems, which is in accordance with experimental data [2] and previous simulations [18]. The two quantities change as expected – the enthalpy decreases upon freezing, while the density increases. It is also important that the average temperature remains constant throughout the whole simulation. In a first order phase transition it is expected that there is no change in this property and, hence, the constant temperature profile serves as an additional validation of the simulations. It ensures also that the simulations are carried out at quasi-equilibrium conditions. The combined behaviour of the three properties may be used as a reliable fingerprint of a phase transition during MD simulations.

The enthalpy changes of the phase transition are collected in Table 1. To calculate them for the two model systems, the difference between the enthalpies of the isotropic liquid and the ordered system (denoted with a green arrow in Fig. 3B) was taken. Cholakova et al. [13] show that 65–75 % of the total phase transition enthalpy is due to the formation of a rotator phase. In most cases, our calculated data are in the range of 71 % to 82 % of the experimental total enthalpy change. Thus, the systems we obtain in the simulations are in rotator phase or they are transitioning from rotator to a crystal phase, according to the enthalpy changes.

Table 1
Enthalpies of the phase transitions (ΔH) observed during the MD simulations; T_i and T_f denote the initial and final temperature, respectively; experimental data [13] are given for comparison.

System	$T_i \rightarrow T_f$, K	ΔH, J/g	$\frac{\Delta H}{\Delta H_{exp}}$, %
Experimental (liquid to triclinic)		236	100
Bulk HEX	300 → 273 K	188	80
	300 → 275 K	170	72
	300 → 278 K	193	82
	350 → 273 K	168	71
HEX/Surf/water	300 → 278 K	184	78
	350 → 273 K	182	77

The density profiles of all simulated systems are presented in Fig. 4. Freezing is observed in both types of models when the temperature is 278 K or lower. This comparison shows that the presence of the surfactant/water interface does not change the freezing point, which corresponds qualitatively to the experimental data [13]. However, there is a quantitative difference of the freezing point obtained from the simulations compared to the experimental value of bulk HEX (291.32 K) [13]. This difference can stem from two reasons. One of them is the supercooling of the system due to its nanoscopic size [13]. The second one might be a tendency of the force field to lower the phase transition temperature. Such an effect was reported for lipid-containing systems modeled with CHARMM36 [62]. In order to check this, we simulated the HEX/Surf/water model at 289 K (which is just slightly below the experimental freezing point of this system), however, with a nucleation seed (several ordered molecules) already present in the initial configuration. The system froze at this temperature, forming a single crystallite. Hence, we can conclude that the lower freezing points in our simulations are a direct result of supercooling, due to the nano-dimensions of the simulated systems. The quantitative deviation of the freezing point, however, should not influence the target properties of the current study. It should be noted that the spontaneous (without any artificial restraints or bias applied) freezing phase transition is observed consistently in the current study with a classical all-atom force field containing all essential bonded and non-bonded terms, and relatively long-time (10^2 ns) effects are quantified. Such a result has not been reported so far for simulations of *n*-alkanes with even number of carbon atoms.

After freezing, a jump of ~ 100 kg/m^3 in the density of the system is observed. This is again common for both types of models since similar reorganization processes take place therein.

The temperature profiles of the liquid systems show that they have equilibrium behaviour after 5 ns both at 350 K and at 300 K. Hence, both trajectories were used to generate starting structures for the cooling. The systems were cooled down to several temperatures, the lowest being 273 K. This cooling resulted in freezing of the system, irrespective of the type of model or the starting temperature (Fig. 4). Since transition from liquid to ordered phase was first observed at 278 K, these trajectories of the bulk HEX and HEX/Surf/water were further simulated to 500 ns. The last 100 ns of the extended trajectories were used for the structural analyses.

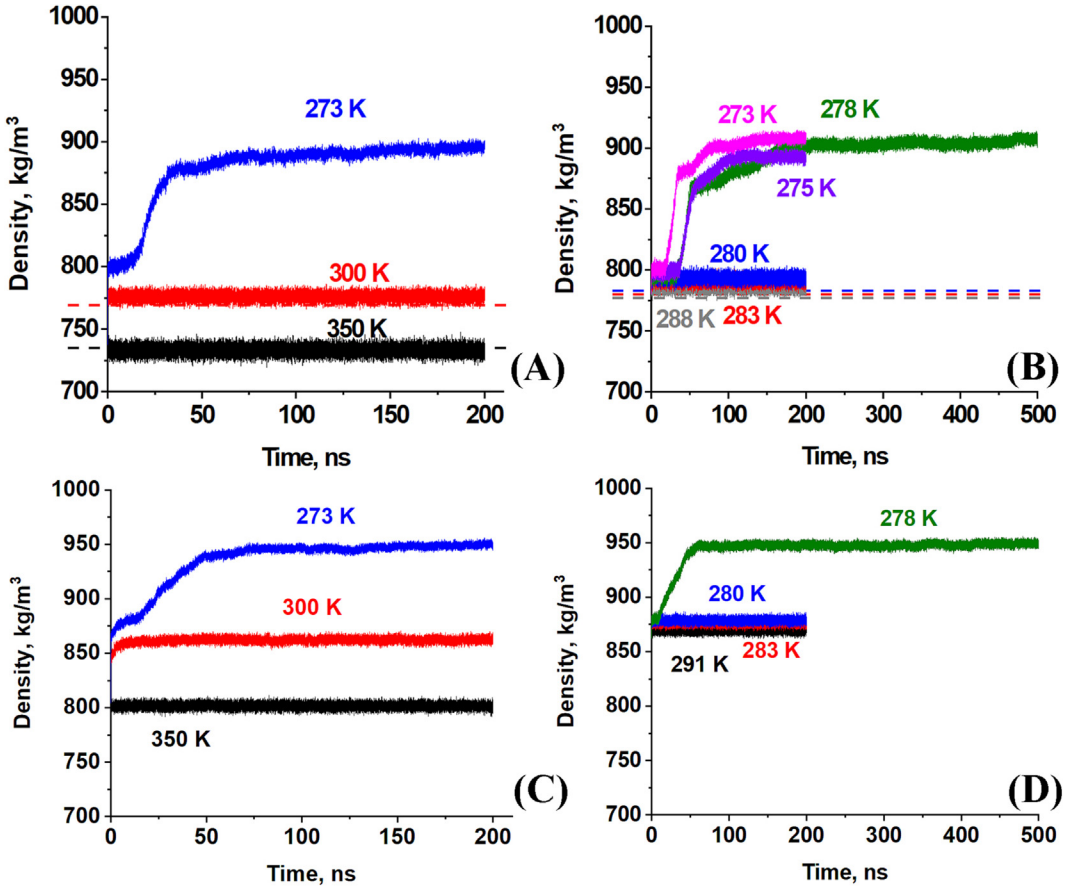

Fig. 4. Mass density as a function of time for (A) bulk HEX and (C) HEX/Surf/water at 300 K, at 350 K and cooled from 350 K to 273 K; (B) bulk HEX and (D) HEX/Surf/water cooled from 300 K to different temperatures; the dashed lines represent the experimental data.

6. Nucleation analysis

The first structural analysis on the model systems aims at identifying the onset of freezing and the molecules forming the nucleation seed. This analysis was achieved by measuring the distance between the atoms 3 and 14 (Fig. 1A) of each alkyl chain throughout the trajectory. When the magnitude of this distance in a molecule reaches 1.4 nm, the alkyl chain is considered frozen. This limiting distance value was chosen to correspond to a molecule in *all-trans* conformation because it is known that alkanes stretch when they freeze [8]. The start of the freezing process was also confirmed by analysing the evolution of the tilt angle of the molecules in the first crystallite formed in each system and mapping it onto the density profile. Analysis of the average tilt angle of the molecules around the time of freezing managed to verify the location of the nucleation site in the systems (Fig. 5B, 5F).

Fig. 5 summarises all described nucleation analyses for bulk HEX and HEX/Surf/water. In accordance with the distance measurement, a moment around 33 ns was determined to be the start of the freezing process for bulk HEX. This matches the rest of the analyses. Comparing the evolutions of the density and the tilt angle shows the same period for the phase transition, which for bulk HEX was ∼ 15 ns long. Assessing the average tilt angle of the molecules in this interval successfully distinguishes the molecules of the nucleation site (marked in grey in Fig. 5B) from the rest. These molecules are identified by the much smaller standard deviation of ca. ± 4°, which illustrates their lowered mobility due to inclusion into the seed. For the HEX/Surf/water system, the freezing starts at ∼ 9 ns according to the distance measurement and the time interval for completion of the phase transition is ∼ 50 ns. Evolution of the density (Fig. 5G) is in agreement with the latter statement. Systematic reduction in the tilt angle (starting at ≈3 ns; Fig. 5E) is observed shortly before the global change in mass density.

Comparison between the average tilt angles of the molecules in the first crystallites of the two systems portrays two types of nucleation (Fig. 5B and 5F). In bulk HEX, the molecules of the seed are in close proximity in space (Fig. 5B), which is an example of homogeneous nucleation [75]. Contrary, in HEX/Surf/water the molecules that are first frozen during the transition are dispersed along the entire length of the crystallite. This is due to the neighbouring surfactant surface, which had already frozen at 300 K and serves as a template [75]. This is in perfect coincidence with known fundamentals of crystallization for these two types of systems. This analysis also extends significantly the molecular-level knowledge of nucleation mechanisms of *n*-alkanes, which was touched only briefly in the work of Esselink et al. [19].

The results from the nucleation analysis reveal that the devised criteria are accurate enough to single out the molecules of the crystal seed at their time of formation, irrespective of the type of the model system. The procedure allows also determining the position of the nucleation site.

7. Overall structuring of the frozen systems

Visual inspection of the trajectories after completion of the phase transition revealed polycrystalline structure of the frozen samples in both model systems. This is illustrated in Fig. 6 where each crystallite is colour-coded. A small fraction of the molecules both in bulk HEX (<3 %) and in HEX/Surf/water (<7.5 %) remained unstructured and were trapped in-between the ordered layers for the duration of the simulations. This observation indicates that the process of intermolecular organization is still ongoing. The latter is valid also for the frozen assemblies. The separate crystallites vary in size and even visually some of them are more ordered than others. Crystallite 2 in bulk HEX and crystallite 1 in HEX/Surf/water are the largest ones in the respective model system. The former contains 60 % of all molecules and the latter – 36 % of the organic fraction. It is noteworthy that these two crystallites are also the ones where the first seed for crystallization was formed.

To characterise the structuring of the frozen part of the systems, the crystallites had to be separated and each of them analysed individually. This prompted the need to devise a methodology to automate the process of identifying and isolating the crystallites. The procedure is described in the Supporting Information, Section: Isolation of crystallites from a polycrystalline system.

To analyse the global structure of each crystallite, radial distribution functions (RDFs) between the centres of mass of the molecules therein were calculated. Fig. 7 contains comparative graphs of the RDFs of the largest crystallite in each of the two model systems and those of reference crystals in triclinic phase and in orthorhombic rotator phase. The data for the reference crystals were obtained from separate MD simulations of the two regular structures which are known for hexadecane. One of them is an ideal triclinic crystal (Fig. S6A) which is the thermodynamically most stable phase for solid hexadecane [13]. The second one (Fig. S6B) is a R_I rotator phase detected experimentally for HEX at surfactant-stabilised interfaces [13]. It features a face-centred orthorhombic lattice with crystallographically determined parameters. These two regular crystals were used as templates for comparison that would allow determining the type of solid-state structure, which had occurred in the crystallites of bulk HEX and HEX/Surf/water after freezing.

It is noteworthy pointing out that the reference rotator phase undergoes structural changes after 500 ns (the molecules tilt with respect to the layers eigenplane), corresponding to the initial stages of the rotator-to-triclinic phase transition. This is accompanied by herringbone-type arrangement of pairs of adjacent layers. The onset of the transition process is initiated early in the simulation both in the rotator phase ($R_I \rightarrow T$) and in the orthorhombic crystal ($O \rightarrow T$). Transitions from and to rotator phases were observed also in earlier MD simulations [37,45,47] but not this particular one. The triclinic crystal did not change significantly after 500 ns of simulation (Figure S6).

The superposition of the RDFs of the largest crystallites of bulk HEX and of HEX/Surf/water is done in Figure S7 to the RDF profiles of both initial 'ideal' references, i.e. triclinic crystal and R_I rotator phase, and in Fig. 7 to the curves of the same two systems averaged for the last 100 ns of the reference MD trajectories. As expected, the intensity of the RDF peaks of the reference models diminished during the MD simulation and some of the sharp lines merged into thermally-broadened peaks. The latter effect was more pronounced for the orthorhombic structure. This effect is probably due to the applied random rotation around the long axis of the molecules in the initial structure of the R_I phase, giving the alkanes therein an additional degree of freedom.

Comparing the crystallites in bulk HEX and HEX/Surf/water with the reference crystals shows that the MD-generated crystallites are in a $R_I \rightarrow T$ transition. Even mapping to the initial crystallographic structures (Fig. S7A and S7B) reveals that the RDF profiles of both crystallites are aligned much better with the peaks of the orthorhombic phase than with those of the triclinic crystal. This statement is confirmed by the data averaged from the reference simulations. The RDFs of the frozen crystallites are clearly aligned to the intermediate $R_I \rightarrow T$ pattern (Fig. 7B). In the case of the triclinic crystal, the number and position of the peaks do not correspond to the ones observed in the crystallites. At the same time, there is no such good match to the RDF profile of the $O \rightarrow T$ system (Figure S8).

The respective RDF plots for all other crystallites in the two model systems are summarised and discussed in the Supporting Information, Section: Radial distribution functions (Figures S8-

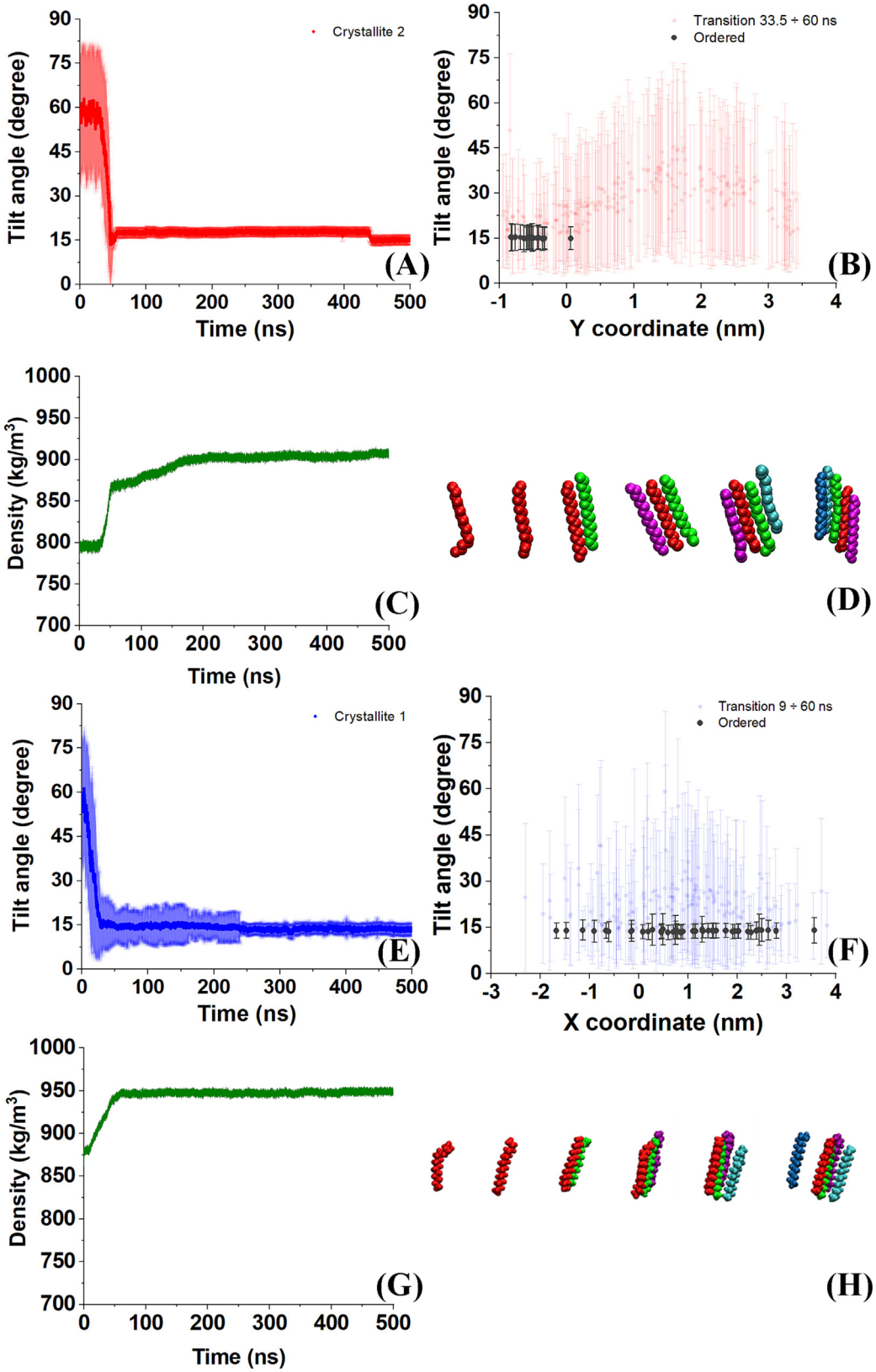

Fig. 5. Summary of the analyses done to determine the onset of freezing and the location of the nucleation site in (A to D) bulk HEX and (E to H) HEX/Surf/water: (A, E) Evolution of the tilt angle of the molecules forming the first crystallite; (B, F) average tilt angle of the molecules in the first crystallite around the time of freezing (33–60 ns in bulk HEX and 9–60 ns in HEX/Surf/water); (C, G) evolution of the density; (D, H) illustration of the first five molecules of the seed.

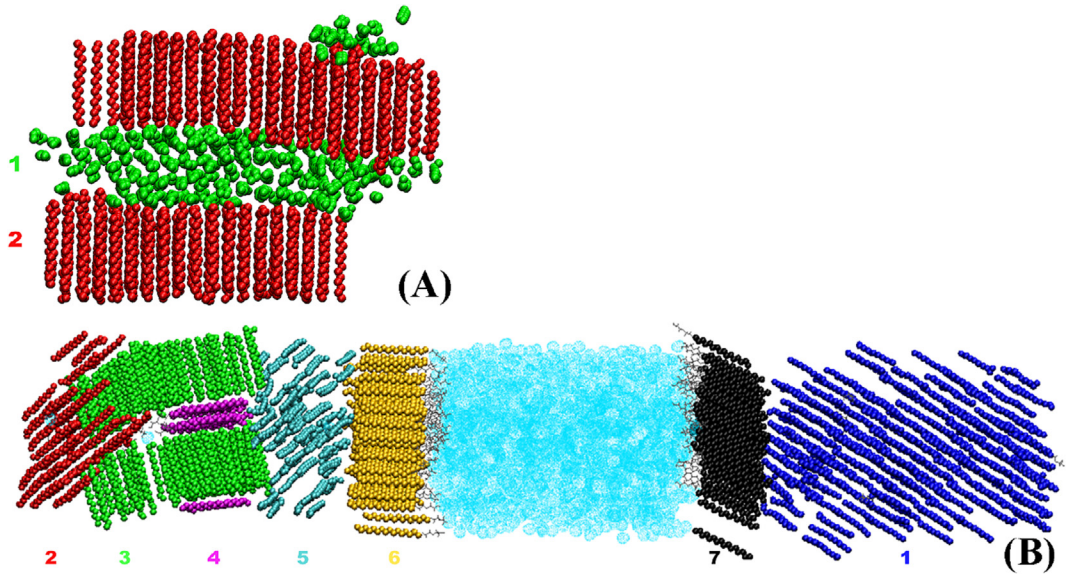

Fig. 6. Illustration of the crystallites in the model systems: (A) bulk HEX and (B) HEX/Surf/water. Each colour represents a unique crystallite formed after cooling from 300 K to 278 K and subsequent 500 ns simulation at 278 K in NPT ensemble.

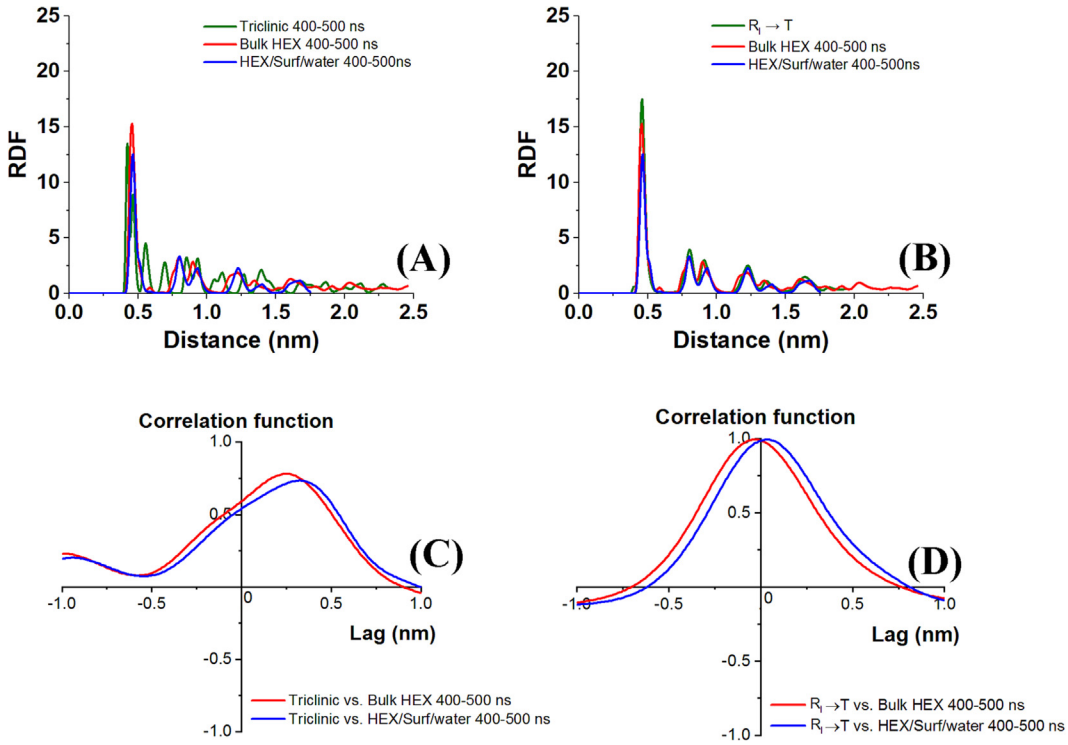

Fig. 7. 3D radial distribution functions between the centres of mass of the aliphatic chains in the largest crystallites of bulk HEX (red) and HEX/Surf/water (blue). They are compared to reference systems of (A) bulk HEX in triclinic phase after 500 ns MD simulation; (B) bulk HEX in orthorhombic rotator phase after 500 ns MD simulation. In all graphs the reference systems are in olive; all RDFs are normalised to the number of molecules and box volume to allow comparison. Correlation functions of the RDF patterns of the two crystallites with those of the (C) triclinic or (D) $R_I \rightarrow T$ reference systems. (For interpretation of the references to colour in this figure legend, the reader is referred to the web version of this article.)

S10). The main observation is that they are in different stage of transition from a rotator to the triclinic crystal phase, with the process progressing faster at the two surfactant-rich surfaces. Another alternative is that the molecules at the surfaces have different, e.g. hexagonal, packing because of the abundance of surfactant there [13].

It should also be noted that the rotator-to-crystal transient phase is obtained both for bulk hexadecane and for HEX at the surfactant-stabilised interface. The RDF peaks of the two model systems are practically identical and coincide with those of the reference rotator phase after a 500 ns MD simulation ($R_I \rightarrow T$ transition). This is an important observation providing molecular-level

evidence for the formation of rotator phases upon freezing of hexadecane-containing systems. It is noteworthy that RDFs have been used successfully before to identify solid-to-liquid phase transition of alkanes [47] but not by strict superposition to fingerprint patterns. The current RDF analysis is also more general than the 2D RDFs in the a-b crystal plane analysed in the work of Fujiwara et al. [28].

The fact that the current simulations predict the solid-state systems going through a rotator phase immediately after freezing agrees with the experimental data for hexadecane [2,13], further confirming the validity of the chosen force field. However, this finding is in contrast to the outcome of a recent computational study of Burrows et al. [49]. There, it is stated that CHARMM36 is not able to reproduce the rotator phase upon melting and freezing of hexadecane. The problem in this previous report might be related not to the force field but to the highly non-equilibrium protocol, which was implemented in the framework of equilibrium molecular dynamics. Therefore, probably the rotator phase could not be sampled with CHARMM36 (a force field developed to reproduce steady-state properties) because no equilibrium trajectories were generated and analysed.

In order to quantify the correlation between the respective RDF profiles, cross-correlation functions (CCFs) were computed with the program package TISEAN [76] (Fig. 7C and 7D). The CCFs reveal almost ideal correlation at minor lags between the $R_I \rightarrow T$ transition and the two most ordered crystallites. In contrast, the CCF of the triclinic crystal after 500 ns simulation with bulk HEX and with HEX/Surf/water is smaller in maximum magnitude (ca. 0.8) and the peak is significantly shifted to larger lags. This confirms the qualitative conclusion made above.

8. Local structuring of the alkyl chains and crystallites

Apart from the global ordering of the frozen entities, the local intra- and intermolecular arrangement within the crystallites may be used to discriminate rotator phases. Therefore, several types of local analyses were performed next.

Analysis of the calculated deuterium order parameter of the carbon atoms in the alkyl chains (see Section: Local structuring of the alkyl chains and crystallites of the Supporting Information) shows that the molecules in the crystallites are stretched out. The standard deviations are a very sensitive indicator of the degree of intramolecular mobility and of the extent of ordering of the molecules in the crystallites.

An important order parameter to determine whether a crystallite is in a rotator phase, and in which one, is the tilt angle of the molecules with respect to the plane of the crystallite (Fig. S4B). Fig. 8 shows the evolution of the average tilt angle and the time-averaged tilt angle of each molecule in the respective crystallites. Crystallite 1 of bulk HEX and crystallite 4 of HEX/Surf/water are presented in a separate Figure S13, due to their disordered nature, resulting in high fluctuations of the angle.

Once again, crystallite 2 of bulk HEX and crystallite 1 of HEX/Surf/water feature the most stable average tilt angle (Fig. 8A). In the former, a shift of 2° is observed in the tilt at ~ 430 ns. This shift is accompanied by further ordering in the crystallite, evidenced by smaller standard deviation and discussed in more detail in the Supporting Information, Section: Tilt angle analysis. Temporal separation of the molecular tilts along the trajectory reveals that the transition to a more upright position is a collective process involving all molecules in the crystallite.

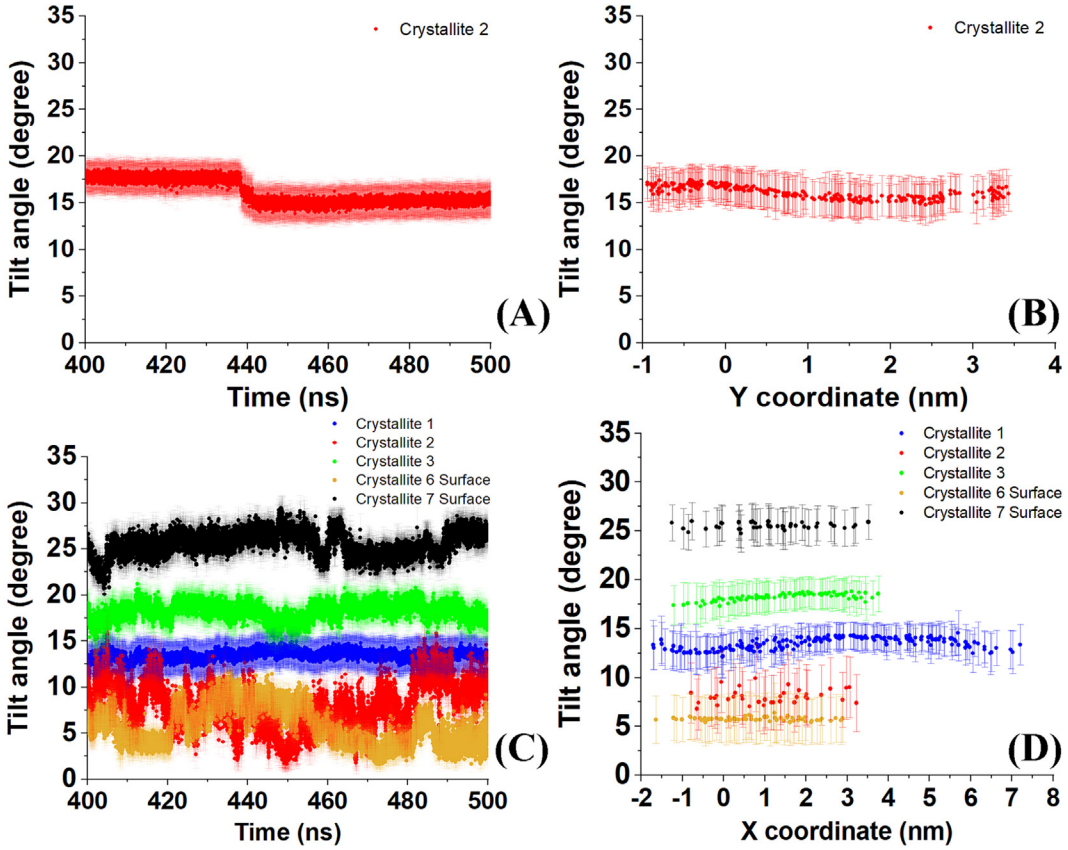

Fig. 8. Evolution of the tilt angle averaged over all molecules with respect to the plane of each crystallite as a function of time in: (A) bulk HEX and (C) HEX/Surf/water. Time-averaged tilt angle of each molecule as a function of its x- or y-coordinate in: (B) bulk HEX and (D) HEX/Surf/water. Only data for the well-structured crystallites of (top) bulk hexadecane and (bottom) hexadecane-surfactant system are shown.

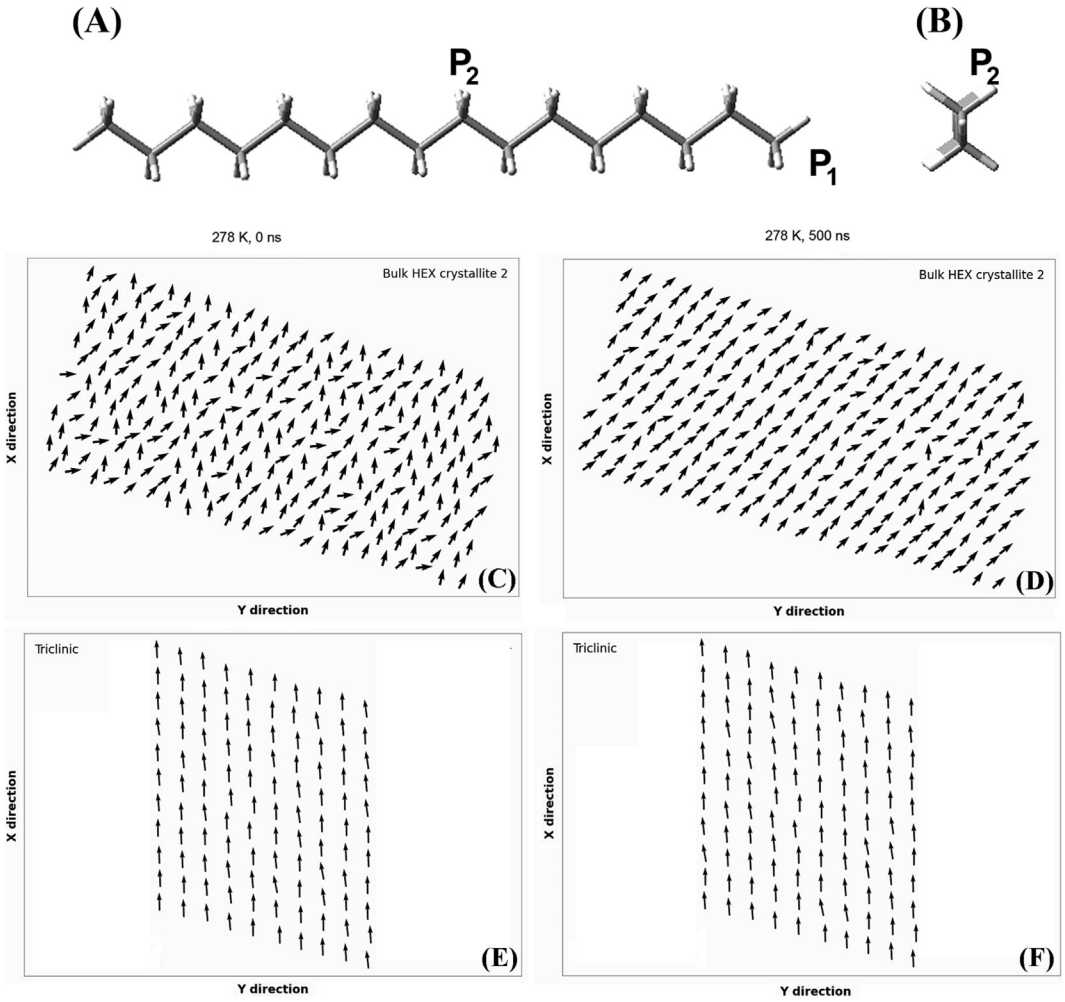

Fig. 9. Illustration of the principal axis P_2 describing the orientation of the molecules in a plane perpendicular to the long molecular axis; views (A) parallel and (B) perpendicular to the long molecular axis of a hexadecane molecule are given; representative orientation of P_2 of each alkane molecule in (middle) crystallite 2 of bulk HEX and (bottom) the reference triclinic crystal: (C) initial liquid state of bulk HEX, (D) final ordered state of bulk HEX, (E) initial and (F) final frame of the reference crystal.

Crystallite 7 of HEX/Surf/water has the largest tilt angle of all crystallites ($\theta_{average}$ = 25°) which supports the assumption from the RDF (Fig. S10E) that transition towards triclinic packing ($\theta_{triclinic}$ = 19.4° [1]) is underway or that different arrangement is operative because of the prevalent surfactant molecules at the surface. It is corroborated also by a previous study of Ryckaert et al. on $C_{23}H_{48}$ [25], where a much smaller tilt angle is reported for the R_I rotator phase. Throughout the 100 ns period, fluctuations with varying duration are observed. This observation suggests that the crystallite is not in its final state yet. Crystallite 6 of this model, in contrast, is characterised by the smallest tilt angle. A periodic fluctuation is observed, indicating that there are two states in dynamic equilibrium with each other. On the other hand, the fluctuations in crystallite 2 of HEX/Surf/water are more random at the beginning and around 480 ns a systematic increase in θ occurs. This increase could indicate a transition towards triclinic phase, which would explain the formation of shoulders in the first peak in the RDF (Fig. 6A and 6F). Crystallite 3 of HEX/Surf/water has a tilt angle closest to a triclinic phase, which periodically fluctuates about an invariant average value. However, the RDF (Fig. 6B and 6G) suggests that it is closer to a rotator phase in structure. This disparity can be due to an ongoing intermolecular reorganization in the transition from rotator to crystal phase.

The average tilt angles of the individual molecules (Figures 8, S12 and S13, right panels) are rather similar along the entire crystallite, which is another verification of the homogeneous intermolecular arrangement. The degree of ordering of the crystallites is reflected very sensitively in the standard deviations. The standard deviation is about 1.5 times larger (4.7°) in crystallite 1 of bulk HEX than in crystallite 2 (ca. 3.4°). Hence, this parameter may be used as a quantitative measure of the ordering degree in the systems studied. In HEX/Surf/water this hierarchy is as follows: crystallite 1 (1.6°) > crystallite 3 (1.7°) > crystallite 7 (1.9°) > crystal lite 6 (2.4°) > crystallite 2 (3.0°) > crystallite 4 (18.2°). The smaller standard deviations in the model with surfactant-stabilised interfaces imply that smaller changes in the structure occur, related to the slower crystallisation process, due to stabilisation of the rotator phase from the surfactant interfaces [13].

9. Voronoi analysis

After calculating the 2D Voronoi tessellation [71,72] of the alkyl chains (Supporting Information, Section: Cross-section between the molecular long axis and the crystallite plane) one can estimate the average distance to the first neighbours in the separate crystallites. This characteristic is another key indicator for the phase state of the crystallites.

Figure S14 presents the average distance to the first neighbours in crystallite 2 of bulk HEX and in crystallite 1 of HEX/Surf/water. They are superimposed on the profiles for the respective average

Table 2
Summary of direct comparisons between the results obtained from the molecular simulations in this work and available experimental data.

MD outcome	Experimental finding	Reference
Excellent agreement of the simulated HEX mass density with the experimental values in the entire temperature range studied, <5% deviation. Decrease of the mass density of liquid HEX upon temperature increase, as expected;	Decrease of the experimentally measured mass density of liquid HEX upon temperature increase	73
Clear stepwise change of enthalpy and mass density in both model systems upon freezing – a signature of first-order transitions	First-order phase transition determined experimentally for freezing of HEX in the bulk and at surfactant-stabilized interfaces	2, 13
Bulk HEX and HEX/Surf/Water freeze at the same temperature; there is a quantitative difference of the freezing point from the experimental value, explained by the nanoscopic size of the modelled system (supercooling)	The freezing point is not changed by the presence of surfactants	13
Crystallization nuclei form along the entire surface of the surfactant layer in HEX/Surf/Water	Surface nucleation in surfactant-stabilized emulsions of hexadecane is observed	16
A transient rotator phase is present in both model systems	Rotator phases are registered by X-ray diffraction in surfactant-stabilized emulsion drops of hexadecane	17
Freezing is accompanied by increased length of the molecules	Alkanes stretch when they freeze	8
The HEX molecules are tilted with respect to the plane of the crystallite in both models	A tilt angle of 19.4° is measured experimentally in HEX triclinic crystals	1

distances in the initial reference triclinic crystal and in the rotator phase and to those averaged for the last 100 ns of the reference MD trajectories. The peaks corresponding to the rotator phase after 500 ns of MD simulation best describe the positions of the first neighbours in the two crystallites (Figure S14D) while the comparison with the triclinic phase (Figure S14C) reveals almost no coincidence, confirming the results obtained from the RDFs. In addition, the profiles of the distances to the nearest neighbours clearly show a distortion intermediate between that typical for a R_I rotator phase (Figure S14B, green line) and a triclinic crystal (Figure S14A, green line). Analysis of the distances to the first neighbours (Figures S15, S16) of the smaller crystallites also support the conclusions made from the rest of the structural analyses.

10. Rotational order in the crystallites

An essential part of the identification of rotator or crystalline phases is the presence of rotation along the long molecular axis [36]. Such random rotation exists in rotator phases, whereas pure crystalline phases have uniform rotational order of all molecules. This rotation may be quantified by calculating the tensor of the moments of inertia. Then, the second principal axis (P_2, Fig. 9) for each molecule in the crystallite reveals the mutual orientation of the molecules in the crystallite in a plane perpendicular to their long axis. This approach was applied successfully for identification of rotator phases in bulk alkanes [43,49].

Representative snapshots showing the intermolecular orientation in bulk HEX when being cooled down to 278 K and further simulated at this temperature are shown in Fig. 9,C-F. Movies visualizing the evolution of the P_2 orientation in crystallite 2 along the entire trajectory of this model system (Movie S1) and in the whole simulation of the reference triclinic crystal (Movie S2) are provided as Supporting Information. One second of the movie corresponds to 4 ns of the trajectory. It should be noted that the vectors representing the P_2 axis of each hexadecane chain are positioned in each frame at the location of the molecule in the last frame of the trajectory. Hence, only the orientation of the vectors should be traced.

In crystallite 2 of bulk HEX (Fig. 9, C, D), a transition from isotropic liquid to an ordered (similar to the crystalline) structure is observed. This is confirmed by the orientation of P_2 in the reference triclinic crystal (Fig. 9, E, F). The evolution of P_2 in both systems (Movies S1, S2) shows occasional flips of the molecules about their long axis. These rotations are much more intensive in the first 60 ns of the bulk HEX simulation, reflecting the fact that the crystalline alignment of the molecules is assisted by a very short-lived rotator phase. As long as the regular translational order of the molecules is achieved, only thermal fluctuations of the P_2 vector are observed until the end of the simulation. Such thermal fluctuations are observed also in the triclinic crystal. However, the magnitude of the rotations is much smaller and the frequency of flips with larger magnitude is practically negligible. This confirms the above conclusions that the molecules in crystallite 2 of bulk HEX are in the stage of final alignment of the crystalline state.

In contrast, crystallite 1 of HEX/Surf/water (Fig. 10, A, B) first undergoes a transition from liquid state to a rotator phase. The same orientation of the molecules with respect to each other as in this rotator state is observed in the reference system of bulk HEX pre-built in rotator phase (Fig. 10, E, F).

Later in the trajectory (at ca. 200 ns), a second transition occurs from the rotator phase to a phase similar to that in crystallite 2 of bulk HEX and in the triclinic crystal. After the second transition, an equilibrium between the two ordered states is established with the crystalline state being prevalent (Movie S3). The first phase formed after freezing resembles very much the structuring of the reference rotator phase crystal (Movie S4). This behaviour of the HEX/Surf/water coincides with the one registered in experiments – longer-living rotator phase than in bulk HEX, followed by rearrangement to a more ordered state. The new insight from the P_2 orientation analysis is that the second transition is a collective process, which needs to be undertaken by many molecules at once.

Such new type of orientational analysis extends on previous works [43,49] by simultaneously employing a rigorously defined physical quantity, eliminating the need for alignment of the crystallite with any of the crystal planes and providing a direct visualisation of the molecular orientation dynamics.

11. Comparison of the theoretical results to experimental data

Direct comparison of the observations in the conducted simulations and analyses and available experimental data is presented in Table 2. This comparison shows that the simulations reproduce rather well qualitatively, and often also quantitatively, the key experimental characteristics of the processes studied. In addition, the simulations provide a comprehensive molecular description of the initial stages of freezing of hexadecane in the bulk and at a surfactant-stabilized interface.

12. Conclusions

In the current study, a computational protocol based on all-atom molecular dynamics was developed, which was first-time able to reproduce effectively the phase transitions in two types

of hexadecane-containing systems both from regular lattice to isotropic liquid upon heating and back to ordered phase upon cooling. Among four tested different atomistic force fields, it was shown that only CHARMM36 was successful in achieving all objectives. Most importantly, this classical potential was able to reproduce the formation of a rotator phase in the model systems upon cooling below the freezing point. The overall good description of the freezing processes was achieved by appropriate combination of the simulation parameters, force field, and sufficiently long equilibrium sampling of the model systems at both end points – liquid and frozen. This allowed gaining several new insights by using the suggested protocol, which represent progress in the field. First, both the melting and the freezing of the systems are modeled, while it is common practice to simulate only melting [32,35,45,47]. Modelling also the freezing allowed determining the onset of freezing and reproducing the experimentally observed polycrystalline structure of both model systems (bulk hexadecane and HEX/Surfactant/water). Extending the parameters used to monitor phase transitions in prior studies [35,46,49], enthalpy was suggested as a sensitive indicator. Up to now, the structure of several solid-state phases mostly of long-chain alkanes was characterized [23] and it was discovered that kinks in the alkyl chains are needed for rotator phases to take place [41,42]. A marked novelty of the current simulations is that the nucleation mechanism was also assessed and quantified by a robust multi-analyses approach. Thereby, a qualitative difference between the two models was witnessed – stochastic and localized seeding in the bulk and nucleation spanning the entire surfactant surface in HEX/Surf/Water. Thus, the knowledge on the freezing mechanism of alkanes, depending on the environment, was enriched. The highlighted mechanisms of freezing, together with all thermodynamic and structural parameters obtained from the simulations, are in very good agreement with known experimental data. For example, the first-order transition is confirmed by differential scanning calorimetry measurements [13]. The presence of a rotator phase in surfactant-stabilized systems is established by x-ray scattering [16]. The simulations yield crystal lattice parameters, which are very close to those determined with x-ray diffraction [13,51]. This agreement validates the devised computational protocol.

Previous reports employ a combination of structural characteristics, such as end-chain defects or gauche–trans conformations [32,39], molecular jumps along the alkyl chain [24,36] and global order parameters [37,38] to describe the phase state of frozen alkanes. In this work, the characterization apparatus is extended with a methodology to separate and individually and more thoroughly analyse each crystallite. The devised procedure is generally applicable to solid-state supramolecular assemblies of linear or quasi-linear molecules. Calculation of the evolution of and the average tilt angle for each molecule relative to the crystallite plane in the first and largest crystallite, combined with determination of the deuterium order parameters of the alkyl chains, calculation of intermolecular radial distribution functions, and Voronoi analysis provided unequivocal assignment of the type and degree of solid-state packing of the molecules. It was observed that the largest and among the most ordered crystallites in both model systems are the ones from which the freezing process started. It was also revealed that the crystallites are in different stages of the freezing process. We conjure that within the time scale of the MD simulations (500 ns), the largest crystallites in bulk HEX and HEX/surfactant/water have started transition from an initially formed more disordered rotator phase to a more regular triclinic crystal. This was confirmed visually by analysis of the orientation of the second principal axis of each molecule, where also a collective nature of this transition was discovered. The advanced degree of ordering achieved after co-existence of the same two types of phases is valid also for the surfactant-rich ($C_{16}(EO)_2$) interfaces.

Overall, this computational study offers a direct illustration of some fundamental principles of colloid and interface science at the microscopic space–time scale, which can be used to optimize the practical application of alkane-containing materials. In perspective, a systematic approach for simulating and for comprehensive characterization of the phase transitions in alkane-containing systems has been developed, which may be used for molecular-level depiction and elucidation of the mechanism and time scale of freezing in a diverse set of soft materials.

CRediT authorship contribution statement

Stoyan Iliev: Investigation, Formal analysis, Writing – original draft, Software. **Sonya Tsibranska:** Investigation, Formal analysis, Writing – original draft, Resources. **Anela Ivanova:** Methodology, Conceptualization, Resources, Supervision, Project administration, Writing – review & editing. **Slavka Tcholakova:** Conceptualization, Validation, Writing – review & editing, Project administration. **Nikolai Denkov:** Conceptualization, Validation, Writing – review & editing, Funding acquisition.

Data availability

Data will be made available on request.

Declaration of Competing Interest

The authors declare that they have no known competing financial interests or personal relationships that could have appeared to influence the work reported in this paper.

Acknowledgements

This study was funded by the Bulgarian Ministry of Education and Science, under the National Research Program "VIHREN", project ROTA-Active (№ KP-06-DV-4/16.12.2019). The main part of the computational time was provided on HPC Piz-Daint, CSCS, Zurich (PRACE ICEI, project ALKOOL - icp009). We acknowledge PRACE for awarding access to the Fenix Infrastructure resources, which are partially funded from the European Union's Horizon 2020 research and innovation programme through the ICEI project under the grant agreement N°. 800858. The rest of the computational time was provided on HPC JURECA, Jülich, Germany (project EUSMI25) via funding from the European Union's Horizon 2020 research and innovation programme under grant agreement N° 731019 (EUSMI).

The authors are very grateful to Mr. Nikola Aleksandrov (Sofia University) for setting up the scripts needed for the Voronoi analysis.

Appendix A. Supplementary material

Supplementary data to this article can be found online at https://doi.org/10.1016/j.jcis.2023.01.126.

References

[1] D. Small, (Ed.), The physical chemistry of lipids. From alkanes to phospholipids. Springer, New York, 1986, ISBN-13: 978-0306417634.
[2] E. Sirota, H. King, D. Singer, H. Shao, Rotator phases of the normal alkanes: An x-ray scattering study, J. Chem. Phys. 98 (1993) 5809–5824, https://doi.org/10.1063/1.464874.
[3] D. Cholakova, K. Tsvetkova, S. Tcholakova, N. Denkov, Rheological properties of rotator and crystalline phases of alkanes, Colloids Surfaces A: Physicochem. Eng. Aspects 634 (2022), https://doi.org/10.1016/j.colsurfa.2021.127926 127926.
[4] J. Yoreo, P. Vekilov, Principles of crystal nucleation and growth, Rev. Mineral Geochem. 54 (2003) 57–93, https://doi.org/10.2113/0540057.

[5] J. Dirksen, T. Ring, Fundamentals of crystallization: kinetic effects on particle size distributions and morphology, Chem. Eng. Sci. 46 (1991) 2389–2427, https://doi.org/10.1016/0009-2509(91)80035-W.
[6] A. Sharma, V. Tyagi, C. Chen, D. Buddhi, Review on thermal energy storage with phase change materials and applications, Renew. Sustain. Energy Rev. 13 (2009) 318–345, https://doi.org/10.1016/j.rser.2007.10.005.
[7] E. Evans, R. Skalak (Eds.), Mechanics and thermodynamics of biomembranes, CRC Press, Boca Raton, 1980, https://doi.org/10.1201/9781351074339. eBook ISBN: 9781351074339.
[8] N. Denkov, S. Tcholakova, I. Lesov, D. Cholakova, S. Smoukov, Self-shaping of oil droplets via the formation of intermediate rotator phases upon cooling, Nature 528 (2015) 392–395, https://doi.org/10.1038/nature16189.
[9] D. Cholakova, N. Denkov, S. Tcholakova, I. Lesov, S. Smoukov, Control of drop shape transformations in cooled emulsions, Adv. Colloid Interface Sci. 235 (2016) 90–107, https://doi.org/10.1016/j.cis.2016.06.002.
[10] D. Cholakova, Z. Valkova, S. Tcholakova, N. Denkov, S. Smoukov, "Self-shaping" of multicomponent drops, Langmuir 33 (2017) 5696–5706, https://doi.org/10.1021/acs.langmuir.7b01153.
[11] S. Tcholakova, Z. Valkova, D. Cholakova, Z. Vinarov, I. Lesov, N. Denkov, S. Smoukov, Efficient self-emulsification via cooling-heating cycles, Nat. Commun. 8 (2017) 15012, https://doi.org/10.1038/ncomms15012.
[12] Z. Valkova, D. Cholakova, S. Tcholakova, N. Denkov, S. Smoukov, Mechanisms and control of self-emulsification upon freezing and melting of dispersed alkane drops, Langmuir 33 (2017) 12155–12170, https://doi.org/10.1021/acs.langmuir.7b02048.
[13] D. Cholakova, N. Denkov, Rotator phases in alkane systems: in bulk, surface layers and micro/nano-confinements, Adv. Colloid interface Sci. 269 (2019) 7–42, https://doi.org/10.1016/j.cis.2019.04.001.
[14] E. Sirota, A. Herhold, Transient phase-induced nucleation, Science 283 (1999) 529–532, https://doi.org/10.1126/science.283.5401.529.
[15] M. Broadhurst, An analysis of the solid phase behavior of the normal paraffins, J. Res. Natl. Bur. Stand. sect. A 66A (1962) 241–249.
[16] Y. Shinohara, N. Kawasaki, S. Ueno, I. Kobayashi, M. Nakajima, Y. Amemiya, Observation of the transient rotator phase of n-hexadecane in emulsified droplets with time-resolved two-dimensional small- and wide-angle X-ray scattering, Phys. Rev. Lett. 94 (2005), https://doi.org/10.1103/PhysRevLett.94.097801 097801.
[17] Y. Shinohara, T. Takamizawa, S. Ueno, K. Sato, I. Kobayashi, M. Nakajima, Y. Amemiya, Microbeam X-ray diffraction analysis of interfacial heterogeneous nucleation of n-hexadecane inside oil-in-water emulsion droplets, Cryst. Growth Des. 8 (2008) 3123–3126, https://doi.org/10.1021/cg701018x.
[18] P. Mukherjee, Phase transitions among the rotator phases of the normal alkanes: a review, Phys. Rep. 588 (2015) 1–54, https://doi.org/10.1016/j.physrep.2015.05.005.
[19] K. Esselink, P. Hilbers, B. van Beest, Molecular dynamics study of nucleation and melting of n-alkanes, J. Chem. Phys. 101 (1994) 9033–9041, https://doi.org/10.1063/1.468031.
[20] S. Whittington, D. Chapman, Monte Carlo study of rotational premelting in crystals of long chain paraffins, Trans. Faraday Soc. 61 (1965) 2656–2660, https://doi.org/10.1039/TF9656102656.
[21] M. Mazo, E. Oleynilk, N. Balabaev, L. Lunevskaya, A. Grivtsov, Molecular dynamic simulation of motion in solid polymers. Rotator phase of n-alkane, Polym. Bull. 12 (1984) 303–309, https://doi.org/10.1007/BF00263143.
[22] M. Klein, Computer simulation studies of solids, Ann. Rev. Phys. Chem. 36 (1985) 525–548, https://doi.org/10.1146/annurev.pc.36.100185.002521.
[23] J.-P. Ryckaert, M. Klein, Translational and rotational disorder in solid n-alkanes: Constant temperature-constant pressure molecular dynamics calculations using infinitely long flexible chains, J. Chem. Phys. 85 (1986) 1613–1620, https://doi.org/10.1063/1.451203.
[24] J.-P. Ryckaert, M. Klein, I. McDonald, Disorder at the bilayer interface in the pseudohexagonal rotator phase of solid n-alkanes, Phys. Rev. Lett. 58 (1987) 698–701, https://doi.org/10.1103/PhysRevLett.58.698.
[25] J.-P. Ryckaert, I. McDonald, M. Klein, Disorder in the pseudohexagonal rotator phase of n-alkanes: molecular-dynamics calculations for tricosane, Mol. Phys. 67 (1989) 957–979, https://doi.org/10.1080/00268978900101561.
[26] J.-P. Ryckaert, M. Klein, I. McDonald, Computer simulations and the interpretation of incoherent neutron scattering experiments on the solid rotator phases of long-chain alkanes, Mol. Phys. 83 (1994) 439–458, https://doi.org/10.1080/00268979400101361.
[27] R. Martonak, W. Paul, K. Binder, Orthorhombic phase of crystalline polyethylene: a Monte Carlo study, J. Chem. Phys. 106 (1997) 8918–8930, https://doi.org/10.1063/1.473955.
[28] S. Fujiwara, T. Sato, Molecular dynamics simulation of structure formation of short chain molecules, J. Chem. Phys. 110 (1999) 9757–9764, https://doi.org/10.1063/1.478941.
[29] I.-E. Mavrantza, D. Prentzas, V. Mavrantza, C. Galiotis, Detailed atomistic molecular-dynamics simulation of the orthorhombic phase of crystalline polyethylene and alkane crystals, J. Chem. Phys. 115 (2001) 3937–3950, https://doi.org/10.1063/1.1386912.
[30] W.-N. Shen, P. Monson, Solid-fluid equilibrium in a nonlinear hard sphere triatomic model of propane, J. Chem. Phys. 103 (1995) 9756–9762, https://doi.org/10.1063/1.469939.
[31] A. Malanoski, P. Monson, The phase behavior of a hard sphere chain model of a binary n-alkane mixture, J. Chem. Phys. 112 (2000) 2870–2877, https://doi.org/10.1063/1.480861.
[32] T. Phillips, S. Hanna, Simulations of the mobile phase of polyethylene, Polymer 46 (2005) 11035–11050, https://doi.org/10.1016/j.polymer.2005.09.019.
[33] T. Yamamoto, Computer simulation of the crystal/melt interface in n-alkane with implication for polymer crystallization, J. Chem. Soc., Faraday Trans. 91 (1995) 2559–2564, https://doi.org/10.1039/FT9959102559.
[34] M. Cao, P. Monson, Solid-fluid and solid-solid phase equilibrium in a model of n-alkane mixtures, J. Chem. Phys. 120 (2004) 2980–2988, https://doi.org/10.1063/1.1637332.
[35] M. Cao, P. Monson, Solid-fluid and solid-solid equilibrium in hard sphere united atom models of n-alkanes: Rotator phase stability, J. Phys. Chem. B 113 (2009) 13866–13873, https://doi.org/10.1021/jp902887w.
[36] A. Marbeuf, R. Brown, Molecular dynamics in n-alkanes: Premelting phenomena and rotator phases, J. Chem. Phys. 124 (2006) 054901-1-9. doi: 10.1063/1.2148909.
[37] N. Wentzel, S. Milner, Crystal and rotator phases of n-alkanes: a molecular study, J. Chem. Phys. 132 (2010) 044901-1-10. doi: 10.1063/1.3276458.
[38] N. Wentzel, S. Milner, Simulation of multiple ordered phases in $C_{23}H_{48}$ n-alkane, J. Chem. Phys. 134 (2011) 224504-1-11. doi: 10.1063/1.3589417.
[39] S. Milner, N. Wentzel, Twist solitons in ordered phases of n-alkanes, Soft Matter 7 (2011) 7477–7492, https://doi.org/10.1039/C1SM05326D.
[40] E. Zubova, N. Balabaev, A. Musienko, E. Gusarova, M. Mazo, L. Manevitch, A. Berlin, Simulation of melting in crystalline polyethylene, J. Chem. Phys. 136 (2012) 224906-1-12. doi: 10.1063/1.4728112.
[41] F. Frank, J. van der Merwe, One-dimensional dislocations: static theory, Proc. R. Soc. London, Ser. A 198 (1949) 205–216, https://doi.org/10.1098/rspa.1949.0095.
[42] D. Doherty, A. Hopfinger, Molecular modeling of polymers: molecular dynamics simulation of the rotator phase of C21H44, Phys. Rev. Lett. 72 (1994) 661–664, https://doi.org/10.1103/PhysRevLett.72.661.
[43] F. Guillaume, J. Ryckaert, V. Rodriguez, L. Mac Dowell, P. Girard, A. Dianoux, Molecular dynamics in solid n-nonadecane: Experiments and computer simulations, Phase Transit. 76 (2003) 823–830, https://doi.org/10.1080/01411590310001613707.
[44] D. Tobias, K. Tu, M. Klein, Assessment of all-atom potentials for modeling membranes: molecular dynamics simulations of solid and liquid alkanes and crystals of phospholipid fragments, J. Chim. Phys. Phys.-Chim. Biol. 94 (1977) 1482–1502, https://doi.org/10.1051/jcp/1997941482.
[45] Z. Rao, S. Wang, F. Peng, Self diffusion and heat capacity of n-alkanes based phase change materials: a molecular dynamics study, Int. J. Heat Mass Transf. 64 (2013) 581–589, https://doi.org/10.1016/j.ijheatmasstransfer.2013.05.017.
[46] Z. Rao, S. Wang, Y. Zhang, Molecular dynamics simulations of phase transition of n-nonadecane under high pressure, Phase Transit. 85 (2012) 400–408, https://doi.org/10.1080/01411594.2011.634331.
[47] Y. Tsuchiya, H. Hasegawa, T. Iwatsubo, Prediction of the melting point of n-alkanes using the molecular dynamics method, J. Chem. Phys. 114 (2001) 2484–2488, https://doi.org/10.1063/1.1338508.
[48] Y. Tsuchiya, H. Hasegawa, T. Iwatsubo, Prediction of the latent heat of n-alkanes using the molecular dynamics method, J. Appl. Phys. 42 (2003) 6508, https://doi.org/10.1143/JJAP.42.6508.
[49] A. Burrows, I. Korotkin, A. Smoukov, E. Boek, A. Karabasov, Benchmarking of molecular dynamics force fields for solid–liquid and solid–solid phase transitions in alkanes, J. Phys. Chem. B 125 (2021) 5145–5159, https://doi.org/10.1021/acs.jpcb.0c07587.
[50] M. Bratek, A. Wójcik-Augustyn, A. Kania, J. Majta, K. Murzyn, Condensed phase properties of n-pentadecane emerging from application of biomolecular force fields, Acta Biochim. Polon. 67 (2020) 309–318, https://doi.org/10.18388/abp.2020_5414.
[51] S. Craig, G. Hastie, K. Roberts, J. Sherwood, Investigation into the structures of some normal alkanes within the homologous series C13H28 to C60H122 using high-resolution synchrotron X-ray powder diffraction, J. Mat. Chem. 4 (1994) 977–981, https://doi.org/10.1039/JM9940400977.
[52] G. Bussi, D. Donadio, M. Parrinello, Canonical sampling through velocity rescaling, J. Chem. Phys. 126 (2007), https://doi.org/10.1063/1.2408420 014101.
[53] H. Berendsen, J. Postma, W. van Gunsteren, A. DiNola, J. Haak, Molecular dynamics with coupling to an external bath, J. Chem. Phys. 81 (1984) 3684–3690, https://doi.org/10.1063/1.448118.
[54] G. Tardajos, M. Diaz Peña, E. Aicart, Speed of sound in pure liquids by a pulse-echo-overlap method, J. Chem. Thermodyn. 18 (1986) 683–689.
[55] M. Parrinello, A. Rahman, J. Appl. Phys. 52 (1981) 7182–7190.
[56] D. Frenkel, B. Smit, Understanding Molecular Simulation, Academic Press, San Diego, 2002.
[57] T. Darden, D. York, L. Pedersen, Particle mesh Ewald: An N·log(N) method for Ewald sums in large systems, J. Chem. Phys. 98 (1993) 10089–10092, https://doi.org/10.1063/1.464397.
[58] U. Essmann, L. Perera, M. Berkowitz, T. Darden, H. Lee, L. Pedersen, A smooth particle mesh Ewald method, J. Chem. Phys. 103 (1995) 8577–8593, https://doi.org/10.1063/1.470117.
[59] A. Toukmaji, C. Sagui, J. Board, T. Darden, Efficient PME-based approach to fixed and induced dipolar interactions, J. Chem. Phys. 113 (2000) 10913–10927, https://doi.org/10.1063/1.1324708.
[60] J.-P. Ryckaert, G. Ciccotti, H. Berendsen, Numerical integration of the cartesian equations of motion of a system with constraints: molecular dynamics of n-alkanes, J. Comput. Phys. 23 (1977) 327–341, https://doi.org/10.1016/0021-9991(77)90098-5.

[61] S. Miyamoto, P. Kollman, Settle: An analytical version of the SHAKE and RATTLE algorithm for rigid water models, J. Comput. Chem. 13 (1992) 952–962, https://doi.org/10.1002/jcc.540130805.
[62] J. Klauda, R. Venable, J. Freites, J. O'Connor, D. Tobias, C. Mondragon-Ramirez, I. Vorobyov, A. MacKerell Jr., R. Pastor, Update of the CHARMM All-atom additive force field for lipids: validation on six lipid types, J. Phys. Chem. B 114 (2010) 7830–7843, https://doi.org/10.1021/jp101759q.
[63] (a) C.J. Dickson, B.D. Madej, Å.A. Skjevik, R.M. Betz, K. Teigen, I.R. Gould, R.C. Walker, Lipid14: The Amber Lipid Force Field, J. Chem. Theory Comput. 10 (2014) 865–879;
(b) B. Madej, I. Gould, R. Walker, A parameterization of cholesterol for mixed lipid bilayer simulation within the Amber Lipid14 force field, J. Phys. Chem. B 119 (2015) 12424–12435, https://doi.org/10.1021/acs.jpcb.5b04924.
[64] W. Cornell, P. Cieplak, C. Bayly, I. Gould, K. Merz, D. Ferguson, D. Spellmeyer, T. Fox, J. Caldwell, P. Kollman, A second generation force field for the simulation of proteins, nucleic acids, and organic molecules, J. Am. Chem. Soc. 117 (1995) 5179–5197, https://doi.org/10.1021/ja00124a002.
[65] W. Jorgensen, D. Maxwell, J. Tirado-Rives, Development and testing of the OPLS all-atom force field on conformational energetics and eroperties of erganic liquids, J. Am. Chem. Soc. 118 (1996) 11225–11236, https://doi.org/10.1021/ja9621760.
[66] W. Jorgensen, J. Chandrasekhar, J. Madura, R. Impey, M. Klein, Comparison of simple potential functions for simulating liquid water, J. Chem. Phys. 79 (1983) 926–935, https://doi.org/10.1063/1.445869.
[67] W. Jorgensen, J. Madura, Temperature and size dependence for Monte Carlo simulations of TIP4P water, Mol. Phys. 56 (1985) 1381–1392, https://doi.org/10.1080/00268978500103111.
[68] S.W.I. Siu, K. Pluhackova, R.A. Böckmann, Optimization of the OPLS-AA force field for long hydrocarbons, J. Chem. Theory Comput. 8 (2012) 1459–1470, https://doi.org/10.1021/ct200908r.
[69] M. Abraham, T. Murtola, R. Schulz, S. Páll, J. Smith, B. Hess, E. Lindahl, GROMACS: High performance molecular simulations through multi-level parallelism from laptops to supercomputers, Software X 1–2 (2015) 19–25, https://doi.org/10.1016/j.softx.2015.06.001.
[70] W. Humphrey, A. Dalke, K.V.M.D. Schulten, Visual molecular dynamics, J. Mol. Graph. 14 (1996) 33–38, https://doi.org/10.1016/0263-7855(96)00018-5.
[71] F. Aurenhammer, Voronoi Diagrams – a survey of a fundamental geometric data structure, ACM Computing Surveys 23 (1991) 345–405, https://doi.org/10.1145/116873.116880.
[72] A. Okabe, B. Boots, K. Sugihara, S. Chiu, D. Kendall, Spatial Tessellations: Concepts and Applications of Voronoi Diagrams, 2nd ed., Wiley, New York, 2000.
[73] S. Outcalt, A. Laesecke, T.J. Fortin, Density and speed of sound measurements of hexadecane, J. Chem. Thermodyn. 42 (2010) 700–706, https://doi.org/10.1016/j.jct.2010.01.003.
[74] A.D. Glova, I.V. Volgin, V.M. Nazarychev, S.V. Larin, S.V. Lyulin, A.A. Gurtovenko, Toward realistic computer modeling of paraffin-based composite materials: critical assessment of atomic-scale models of paraffins, RSC Adv. 9 (2019) 38834–38847.
[75] E. Mura, Y. Ding, Nucleation of melt: From fundamentals to dispersed systems, Adv. Colloid Interf. Sci. 289 (2021), https://doi.org/10.1016/j.cis.2021.102361. doi: 10.1039/c9ra07325f 102361.
[76] R. Hegger, H. Kantz, T. Schreiber, Practical implementation of nonlinear time series methods: The TISEAN package, CHAOS 9 (1999) 413–435, https://doi.org/10.1063/1.166424.